

## DIFFERENCES IN THE STRUCTURAL PROPERTIES AND STAR-FORMATION RATES OF FIELD AND CLUSTER GALAXIES AT $Z \sim 1$

REBECCA J. ALLEN<sup>1,3</sup>, GLENN G. KACPRZAK<sup>1</sup>, KARL GLAZEBROOK<sup>1</sup>, KIM-VY H. TRAN<sup>2</sup>, LEE R. SPITLER<sup>3,4</sup>, CAROLINE M. S. STRAATMAN<sup>5</sup>, MICHAEL COWLEY<sup>3,4</sup>, THEMIYA NANAYAKKARA<sup>1</sup>

*Draft version September 21, 2021*

### ABSTRACT

We investigate the dependence of galaxy sizes and star-formation rates (SFRs) on environment using a mass-limited sample of quiescent and star-forming galaxies with  $\log(M_*/M_\odot) \geq 9.5$  at  $\bar{z} = 0.92$  selected from the NMBS survey. Using the GEEC2 spectroscopic cluster catalog and the accurate photometric redshifts from NMBS, we select quiescent and star-forming cluster ( $\bar{\sigma} = 490 \text{ km s}^{-1}$ ) galaxies within two virial radius,  $R_{vir}$ , intervals of  $2 > R_{vir} > 0.5$  and  $R_{vir} < 0.5$ . Galaxies residing outside of  $2 R_{vir}$  of both the cluster centres and additional candidate over-densities are defined as our field sample. Galaxy structural parameters are measured from the COSMOS legacy *HST*/ACS F814W image. The sizes and Sérsic indices of quiescent field and cluster galaxies have the same distribution regardless of  $R_{vir}$ . However, cluster star-forming galaxies within  $0.5 R_{vir}$  have lower mass-normalised average sizes, by  $16 \pm 7\%$ , and a higher fraction of Sérsic indices with  $n > 1$ , than field star-forming galaxies. The average SFRs of star-forming cluster galaxies show a trend of decreasing SFR with clustocentric radius. The mass-normalised average SFR of cluster star-forming galaxies is a factor of  $2 - 2.5$  ( $7 - 9\sigma$ ) lower than that of star-forming galaxies in the field. While we find no significant dependence on environment for quiescent galaxies, the properties of star-forming galaxies are affected, which could be the result of environment acting on their gas content.

### 1. INTRODUCTION

The size growth rate of galaxies is indicative of the mechanisms that drive galaxy evolution. Quiescent galaxies with  $\log(M_*/M_\odot) \sim 11$  have demonstrated an accelerated growth having sizes 4–6 times larger at  $z = 0$  compared to  $z = 2 - 4$ , while star-forming galaxies with similar masses have only grown by a factor of 2 since  $z = 4$  (Morishita et al. 2014; van der Wel et al. 2014; Straatman et al. 2015a).

The dramatic size growth of quiescent galaxies is partly attributed to their decedent nature; some fraction of their population form when already massive star-formers collide in major mergers or quench. Once they have formed, it is thought that the majority of their size growth comes from adiabatic expansion (e.g., Fan et al. 2008, 2010) or minor and major merging events (e.g., Khochfar & Silk 2006; Naab et al. 2009; Guo et al. 2011; Hiltz et al. 2013; McLure et al. 2013; Szomoru et al. 2013). However, studies have shown that the rate of minor mergers at  $z > 1$  is not sufficient to be the dominant means of growth for passive galaxies (Newman et al. 2012; Belli et al. 2014). Therefore, the mechanisms that drive the accelerated growth of quiescent galaxies are still not well understood.

On the other hand, the steady growth of star-forming galaxies is attributed mainly to the production of new stars from cold gas reservoirs and inflowing streams (e.g., L’Huillier et al. 2012; Bouché et al. 2013), and possibly via minor mergers (van Dokkum et al. 2010). While observations and simulations have provided some insight into the channels that drive

galaxy growth, one important aspect is still debated: the role of environment.

At  $z = 0$ , there is a clear relation between the morphology of galaxies and the environment they inhabit (Dressler 1980; Dressler et al. 1997) with elliptical galaxies being more prevalent in high density regions. It has become apparent that as early as  $z = 2 - 3$  these large scale structures began to form (Lemaux et al. 2014, 2012; Spitler et al. 2012). Therefore, the role of environment must be understood to better constrain the instruments that drive galaxy growth.

It is thought that high density environments are efficient at removing the cold gas from star-forming galaxies via galaxy-galaxy interactions, strangulation, and harassment (Gunn & Gott 1972; Moran et al. 2007). The depletion of cold gas and quenching of star-forming galaxies, could stunt their size growth, creating an observable difference between their sizes/star-formation rates and those of field star-forming galaxies. In fact, the star-formation density relation has been observed from  $z \sim 0 - 2$  (e.g., Kauffmann et al. 2004; Patel et al. 2011; Quadri et al. 2012), providing direct evidence that environment is effective at quenching star-forming galaxies.

However, the effects of environment on star-forming galaxies may not be completely destructive. At  $z \geq 1$  the cores of clusters are hosts to galaxies with star-formation rates (SFRs) up to  $\sim 100 M_\odot \text{ yr}^{-1}$  (Cooper et al. 2008; Hilton et al. 2010; Tran et al. 2010; Lemaux et al. 2012). The elevated SFRs of these galaxies could lead to bulge growth and a transformation from late-type morphologies to bulge dominated early-type morphologies. In fact, Mei et al. (2015) have confirmed a substantial population of star-forming early-type galaxies clusters at  $z = 1.84$  and  $z = 1.9$ . The mass-size relation of these cluster galaxies follows that of passive early-type cluster galaxies at  $z \sim 0.7 - 1.5$ . Furthermore, Lang et al. (2014) found that star-forming galaxies with  $\log(M_*/M_\odot) > 11$  have bulge to total ratios (B/T) of 40–50%. Assuming imminent quenching, then significant bulge growth and a transformation

<sup>1</sup> Swinburne University of Technology, Victoria 3122, Australia

<sup>2</sup> George P. and Cynthia Woods Mitchell Institute for Fundamental Physics and Astronomy, and Department of Physics and Astronomy, Texas A&M University, College Station, TX 77843

<sup>3</sup> Australian Astronomical Observatories, PO Box 915, North Ryde, NSW 1670, Australia

<sup>4</sup> Department of Physics & Astronomy, Macquarie University, Sydney, NSW 2109, Australia

<sup>5</sup> Leiden Observatory, Leiden University, P.O. Box 9513, 2300 RA Leiden, The Netherlands

of late-type to early-type is expected for massive star-formers transitioning into quiescence. Therefore, measuring the properties of star-forming galaxies at different cluster radii may provide answers to the level of impact environment plays on their size growth.

Simulations (e.g., [Shankar et al. 2014](#)) indicate a strong dependence of median galaxy size on halo mass with quiescent galaxies in higher mass halos having larger sizes by a factor of  $\sim 1.5-3$ . If quiescent galaxies are undergoing accelerated growth due to higher merger rates in clusters, then a measurable size difference should be present. Therefore, it is important to compare the sizes of quiescent galaxies in different environments to understand if their accelerated growth can be attributed to major merger events.

To date, there are a number of studies that have used a combination of high resolution imaging, multi-band photometry, and spectroscopy to study the stellar mass-size relation as a function of environment. These studies span  $0 \leq z \leq 2$  and show that the effect of environment on the sizes of quiescent galaxies is either weak or non-existent ([Papovich et al. 2012](#); [Bassett et al. 2013](#); [Huertas-Company et al. 2013b,a](#); [Cebrián & Trujillo 2014](#); [Newman et al. 2014](#); [Allen et al. 2015](#); [Kelkar et al. 2015](#)).

There are few studies that have examined the effect of environment on star-forming galaxy sizes up to  $z \sim 2$ . At  $z = 0.12$ , [Cebrián & Trujillo \(2014\)](#) find that field late-type galaxies with  $\log(M_*/M_\odot) \sim 10.3$  are up to 7.5% larger in size than cluster late-type galaxies of similar mass. At  $0.4 < z < 0.8$ , [Kelkar et al. \(2015\)](#) find no significant difference in the sizes of field and cluster late-type galaxies with  $\log(M_*/M_\odot) > 10.2$ . At  $z = 2.1$ , [Allen et al. \(2015\)](#) found that the mass-normalised sizes of star-forming cluster galaxies with  $\log(M_*/M_\odot) \geq 9$ , are 12% larger than their field counterparts. The conflicting results and lack of a strong size difference could be due to an evolution in the SFR-density relation as well as differences in galaxy sample selection.

To understand if there is truly a size dependence on environment, it is important to determine at what epoch these differences emerged and to trace their evolution. However, finding and quantifying environment at  $z \geq 0.8$  is difficult because accurate redshifts are necessary, and spectroscopy becomes time expensive.

The Galaxy Environment Evolution Collaboration 2 (GEEC2) spectroscopic survey ([Balogh et al. 2014](#)) has identified 11 galaxy clusters in the COSMOS field with  $0.8 < z < 1$  ( $\bar{z} = 0.82$ ,  $\bar{\sigma} = 380 \text{ km s}^{-1}$ ). These clusters were found as part of a follow up survey that utilises the spectroscopic catalog of zCOSMOS [Lilly et al. \(2007\)](#) and the X-ray catalog of [George et al. \(2011\)](#). With the use of spectroscopy, [Balogh et al. \(2014\)](#) have confirmed over-densities that can be used to probe the effects of environment on galaxy evolution.

While spectroscopy produces accurate redshifts, it is biased towards bright and/or blue objects. The photometric data obtained from ground based surveys such as the NEWFIRM medium-band Survey (NMBS), can be used to calculate very accurate photometric redshifts, rest-frame colors, stellar masses, SFRs, and other galaxies properties (e.g., [van Dokkum et al. 2010](#); [Kriek et al. 2011](#); [Whitaker et al. 2012b,a](#)). Therefore, it can be used to create more complete samples of both star-forming and quiescent galaxies.

Lastly, it is vital to have high resolution imaging from which to measure the physical properties of galaxies, such as size. Through legacy surveys, such as CANDELS ([Gro-](#)

[gin et al. 2011](#); [Koekemoer et al. 2011](#)), public *HST* imaging provides coverage in multiple wavelengths of several legacy fields. The PSF FWHM of *HST* imaging ranges from  $0.16-0.10''$ , therefore, it is possible to measure galaxy sizes down to  $\sim 0.08-0.05''$  (or  $\sim 0.5 \text{ kpc}$  at  $z = 1$ ) ([van Dokkum et al. 2010](#)).

In this paper, we use both the GEEC2 survey and NMBS to select a mass-complete ( $\log(M_*/M_\odot) \geq 9.5$ ) sample of field and cluster galaxies. For the first time, we compare the structural properties of galaxies as a function of cluster virial radius to quantify where the effects of environment begin. We use the virial radius to determine field, cluster outskirts, and cluster core samples. To understand if environment is affecting the growth of star-forming and quiescent galaxies, we separate galaxies based on their star-formation activity using rest-frame colors. We use *HST*/ACS F814W imaging to measure the structural parameters of our samples of galaxies to compare the mass-size relation and average Sérsic indices of field and cluster, star-forming and quiescent galaxies at  $z \sim 1$ . To complement the mass-size relation, we analyse the average SFRs of our sample to gain additional insight on how galaxy growth may be affected by environment.

The paper is organised as follows: in Section 2 we describe our sample selection and its properties, in Section 3 we describe our construction of the mass-size relation, followed by our results regarding the average sizes, Sérsic indices, and SFRs in Section 4. We discuss the consequences of our findings in Sections 5 and 6. We assume a  $\Lambda$ CDM cosmology with  $\Omega_\Lambda = 0.73$ ,  $\Omega_m = 0.27$ , and  $H_0 = 71 \text{ km s}^{-1}$ .

## 2. SAMPLE

### 2.1. Cluster Locations

We use the GEEC2 spectroscopic survey ([Balogh et al. 2014](#)) to obtain galaxy clusters at  $z \sim 1$ . In the GEEC2 survey, candidate clusters were chosen from the X-ray catalog of [George et al. \(2011\)](#) and from the previous spectroscopic survey zCOSMOS ([Lilly et al. 2007](#)). To confirm the existence of candidate clusters, [Balogh et al. \(2014\)](#) searched for additional galaxy members by obtaining Gemini/GMOS spectra of galaxies with photometric redshifts from [Capak et al. \(2007\)](#) that were consistent with the clusters.

The GEEC2 cluster centres were chosen based on the original X-ray centres of [George et al. \(2011\)](#) and confirmed by the mean location of all spectroscopic members of the cluster. Velocity dispersions were calculated using the spectroscopic members and range between  $350$  and  $690 \text{ km s}^{-1}$ . From the velocity dispersions they calculated the virial radii,  $R_{vir}$ .

We use the cluster centres and virial radii defined by the spectroscopically confirmed galaxies to select our photometric sample of cluster galaxies, which is outlined in Section 2.3.1. For more details regarding cluster centres, velocity dispersions, and their observations, please refer to [Balogh et al. \(2014\)](#).

### 2.2. Photometric Catalog

For our sample of field and cluster galaxies we use NMBS ([Whitaker et al. 2011](#)) to obtain accurate photometric redshifts, stellar masses, rest-frame colors, and star-formation rates (SFRs). As outlined above, NMBS is highly advantageous because it is a deep survey that utilises medium-band photometry that can be well fit by template SEDs, providing very accurate redshifts and galaxy properties, such as mass, SFR, stellar ages, etc., without the use of spectroscopy.

NMBS stellar masses were obtained by fitting stellar population templates to the photometric data using the code FAST (Kriek et al. 2009). Stellar population models were made with the population synthesis code of Bruzual & Charlot (2003) assuming a Chabrier IMF and solar metallicity. Star formation histories were modelled as exponentially decreasing ( $\Psi \propto e^{-t/\tau}$ ) with values of  $\log(\tau/\text{year}) = 7 - 10$  in steps of 0.2 and  $\log(\text{age}/\text{yr}) = 7.6 - 10.1$  in steps of 0.1. NMBS is mass complete down to  $\log(M_*/M_\odot) = 9.5$  at  $z = 1$ . SFRs were derived using UV and IR luminosities, which includes MIPS 24 micron photometry and the rest-frame 2800Å luminosity, and is outlined in Whitaker et al. (2012b). NMBS redshifts and rest-frame colors were determined by fitting template SEDs with the code EAZY (Brammer et al. 2008). The accuracy of the photometric redshifts of NMBS is  $\sigma_z/(1+z) < 0.015$  and we will refer to it as  $\sigma$  for the rest of the paper. For a full outline of the parameters and models that were used in both EAZY and FAST, please see Whitaker et al. (2011).

NMBS has one square degree pointing in the COSMOS and AEGIS fields. For this study we use data that covers COSMOS to match galaxies from GEEC2.

### 2.3. Field and Cluster Sample Selection

#### 2.3.1. Cluster Galaxies

Due to the biases of spectroscopy towards star-forming galaxies, we select galaxies using the accurate photometric redshifts of NMBS ( $\sigma_z/(1+z) = 0.015$ ) instead of using only spectroscopic cluster members from GEEC2. The NMBS footprint differs from that of the GEEC2 survey, therefore, we use three clusters (GEEC2 IDs: 130, 143, and 150) that are situated in both NMBS and GEEC2 footprints. The total number of GEEC2 cluster galaxies in NMBS is 93. The spectroscopic redshift range of the three clusters is  $0.83 - 0.94$  ( $\bar{z} = 0.92$ ).

We select cluster galaxies from the COSMOS (Scoville 2007) field, within  $\pm 4\sigma$  of the spectroscopic redshift of each cluster centre. The  $4\sigma$  selection guarantees that we recover 94% (87/93) of the original GEEC2 spectroscopic cluster members in NMBS using photometric redshifts. We select two cluster samples using  $R_{\text{vir}}$ . We use  $2 > R_{\text{vir}} > 0.5$ , which we refer to as  $2 R_{\text{vir}}$  for the rest of the paper, and  $R_{\text{vir}} < 0.5$ , which we refer to as  $0.5 R_{\text{vir}}$  for the rest of the paper. For massive galaxy haloes,  $M_h \geq 10^{14} M_\odot$ , substantial populations of red galaxies have been observed out to  $2-4R_{\text{vir}}$  (Hansen et al. 2009). Because the cluster haloes of GEEC2 are on the order of  $M_h \sim 10^{13-14} M_\odot$ , we create an outer ( $2 R_{\text{vir}}$ ) cluster sample to understand if environment is affecting the sizes of galaxies at larger radii. The second radius is used to create a core cluster sample that is within  $0.5 R_{\text{vir}}$  of each cluster centre.  $0.5 R_{\text{vir}}$  is generally considered to be the transition radius between the cluster core and outskirts (e.g., Delaye et al. 2014).

The physical sizes of the apertures for the two different selections range  $200 - 100''$  ( $\sim 1.05 - 0.53$  Mpc at  $\bar{z} = 0.92$ ) and  $67 - 33''$  ( $\sim 0.53 - 0.26$  Mpc at  $\bar{z} = 0.92$ ), for  $2 R_{\text{vir}}$  and  $0.5 R_{\text{vir}}$ , respectively. The total fraction of GEEC2 spectroscopically confirmed galaxies that reside in NMBS to our photometrically selected galaxies within these two radii are 42/50 and 37/37 for  $2 R_{\text{vir}}$  and  $0.5 R_{\text{vir}}$ , respectively. The distribution of redshifts for our photometrically selected samples compared to the GEEC2 spectroscopic sample are shown in Figure 1.

We use masses from NMBS to create a mass complete sample by including all galaxies with  $\log(M_*/M_\odot) > 9.5$ . The total number of galaxies in each of our samples is listed in

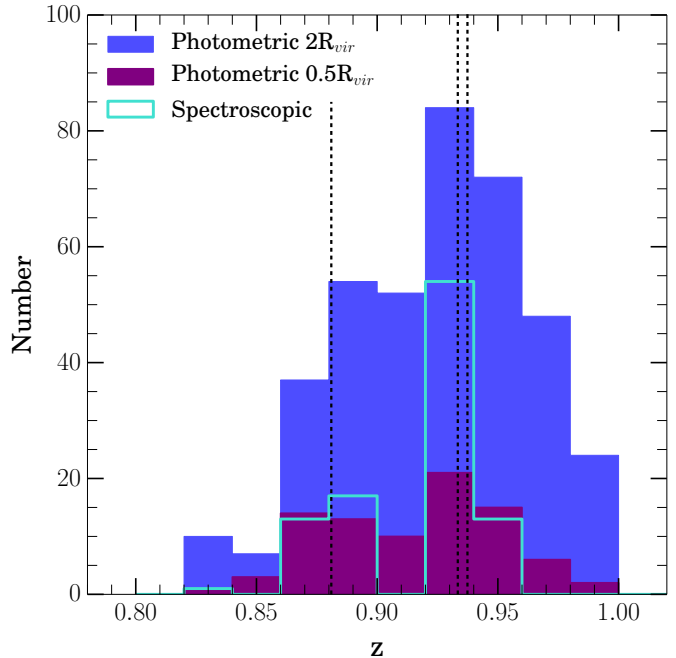


FIG. 1.— The distribution of redshifts for our photometrically selected cluster samples compared to the spectroscopic redshifts of the GEEC2 sample that resides in NMBS. The cluster spectroscopic redshifts are denoted by black dashed lines.

Table 1.

#### 2.3.2. Field Galaxies

The field sample was selected from the COSMOS field using the NMBS photometric redshifts. To locate any other significant over-densities besides the GEEC2 clusters, we use the seventh-nearest-neighbor technique to map the projected density of the COSMOS field within  $0.76 < z < 1.06$ . This redshift range corresponds to  $\pm 8\sigma$  of the lowest and highest spectroscopic cluster centres. The significance of any over-densities is determined by comparing the mean density at  $0.46 \leq z \leq 0.76$  and  $1.06 \leq z \leq 1.36$  to the mean density at  $0.76 < z < 1.06$ .

In Figure 2, we show the seventh-nearest-neighbour projected density map of the COSMOS field at  $0.76 < z < 1.06$  overlaid with the field and cluster samples. The star-forming  $2$  and  $0.5 R_{\text{vir}}$  cluster galaxies, detected for our sample, are shown as solid blue and turquoise diamonds, respectively. The quiescent  $2$  and  $0.5 R_{\text{vir}}$  cluster galaxies, detected for our sample, are shown as solid red and pink circles, respectively. The quiescent field and star-forming galaxies are shown as red open squares and blue open triangles, respectively. We discuss the separation of star-forming and quiescent galaxies in Section 2.4.

Our seventh-nearest-neighbour technique recovers all GEEC2 clusters, and their significance is  $\geq 15\sigma$ . We note that additional over-densities are present in the NMBS field. However, we can neither confirm that these candidate over-densities are actual clusters instead of chance projects, or can adequately characterized them (i.e., determine their  $R_{\text{vir}}$ , velocity dispersions, or halo masses), so we do not include them in our analysis. These extra over-densities, of significance greater than  $15\sigma$ , are shown as red circles in Figure 2. The size of the red circles are taken as the average  $2 R_{\text{vir}}$  of our GEEC2 clusters,  $\sim 230''$ . Our field samples are selected outside of these apertures to ensure that they do not reside in

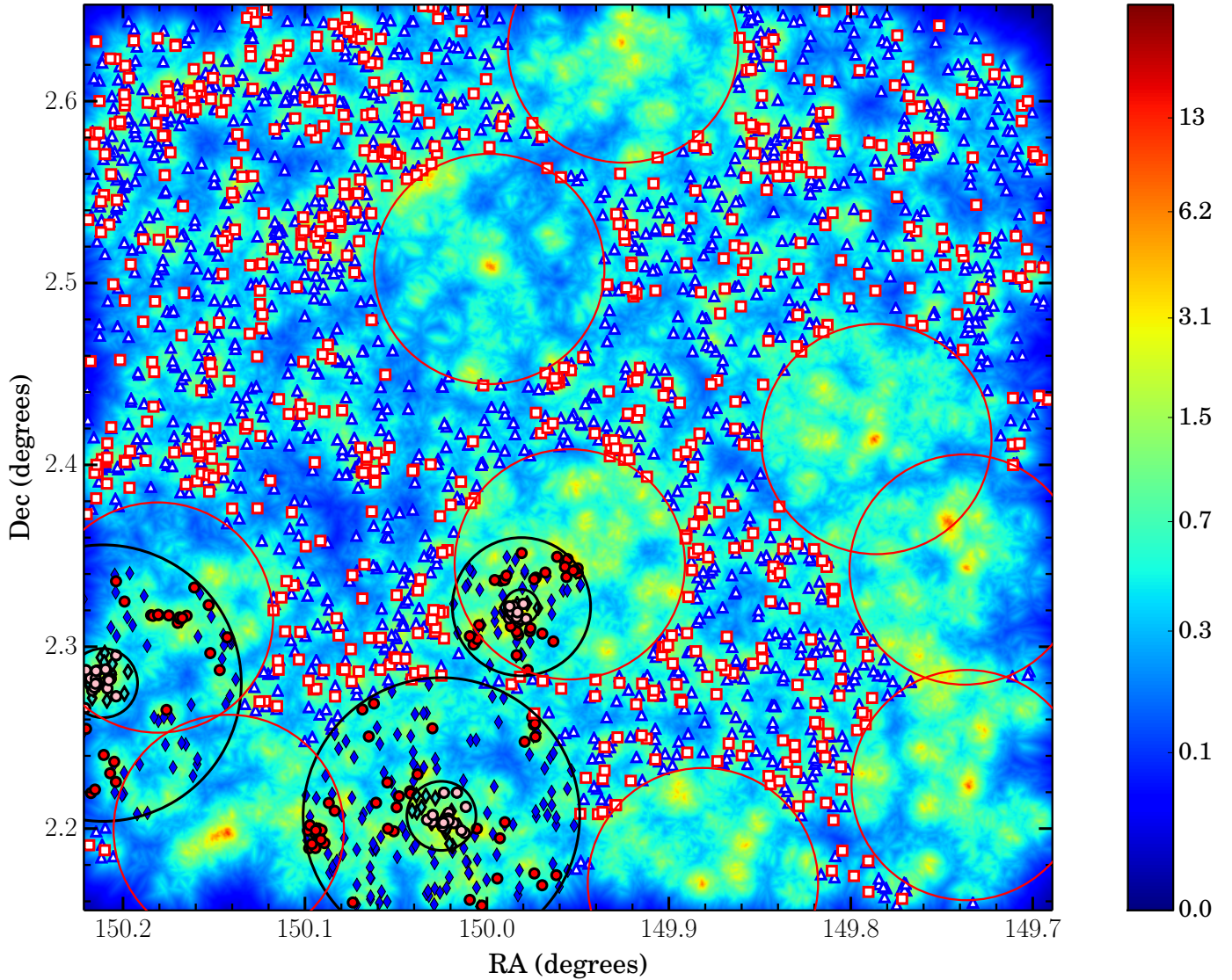


FIG. 2.— Seventh-nearest-neighbor projected density map of the NMBS footprint in the COSMOS field. The color bar represents the significance, in sigma, of the projected density at  $0.76 < z < 1.06$  above the mean density. The mean density is averaged over the field at  $0.46 \leq z \leq 0.76$  and  $1.06 \leq z \leq 1.36$ . Field star-forming galaxies (open blue triangles) and field quiescent galaxies (open red squares) were selected where no significant ( $> 15\sigma$ ) large-scale candidate overdensities were found. These additional overdensities are denoted by red circles, and have radii =  $227''$ . Three galaxy overdensities in the COSMOS field were found in the GEEC2 survey (Balogh et al. 2014), and confirmed using the seventh-nearest-neighbor metric, with photometric redshifts between  $0.821 < z < 1.004$ . The cluster samples are selected within  $2 R_{vir}$  and  $0.5 R_{vir}$ ,  $200-100''$  ( $\sim 1.05-0.53$  Mpc at  $\bar{z}=0.92$ ) and  $67-33''$  ( $\sim 0.53-0.26$  Mpc at  $\bar{z}=0.92$ ), respectively, of each cluster centre (black solid circles). Our samples of  $2 R_{vir}$  cluster star-forming and quiescent galaxies are shown as blue diamonds and red circles, respectively. The  $0.5 R_{vir}$  cluster samples have the same symbols but are a lighter color.

over-dense regions.

We use the redshift bin,  $0.8 \leq z \leq 1$ , to select our field galaxies, which corresponds to  $\pm 4\sigma$  of the lowest and highest spectroscopic redshift of the cluster centres. We use this narrower redshift bin to eliminate any overlap with neighbouring overdensities. We use the same mass limit as for the cluster samples including all galaxies with  $\log(M_*/M_\odot) > 9.5$ . The total number of galaxies in each of our samples is listed in Table 1.

#### 2.4. Separating Quiescent and Star-Forming Galaxies

Due to the known difference in size evolution between star-forming and quiescent galaxies (e.g., van der Wel et al. 2014), it is important to separate these two populations before we can determine their mass–size relations. We use the  $U - V$  versus  $V - J$  rest-frame color-color diagram to sep-

TABLE 1  
SAMPLE SIZES

|              | Field | $2 > R_{vir} > 0.5$ Cluster | $R_{vir} < 0.5$ Cluster |
|--------------|-------|-----------------------------|-------------------------|
| Star-forming | 1189  | 206                         | 38                      |
| Quiescent    | 535   | 97                          | 47                      |

arate quiescent galaxies from star-forming galaxies and not to confuse dusty star-formers as quiescents (e.g., Labbé et al. 2005; Williams et al. 2009; Wuyts et al. 2009; Whitaker et al. 2012a; Wild et al. 2014). The UVJ color-color selection of passive galaxies is particularly efficient at  $z = 1-3$ , where the  $4000\text{\AA}$  break is moving through the medium-band filters. Straatman et al. (2015b, submitted), show an in-depth

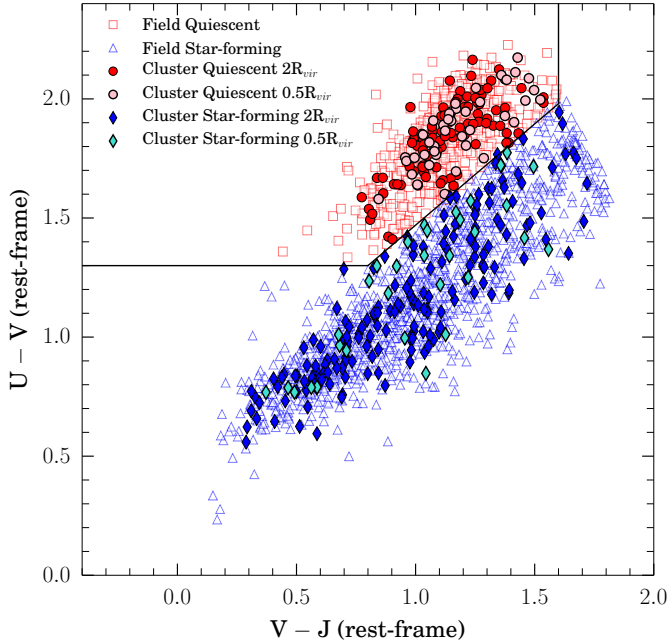


FIG. 3.— Rest-frame  $U - V$  versus  $V - J$  colors for our sample of field and cluster galaxies at  $\bar{z} = 0.92$ . Star-forming cluster (field) galaxies are shown as filled (open) blue diamonds (triangles). Quiescent  $2R_{vir}$  cluster (field) galaxies are shown as filled (open) red circles (squares). The cluster galaxies chosen within  $0.5R_{vir}$  are the same symbol as their  $2R_{vir}$  counter-parts but a lighter color. The black line represents the boundary for quiescent galaxies (above) and star-forming galaxies (below). We use this diagram to separate our sample into star-forming and quiescent galaxies.

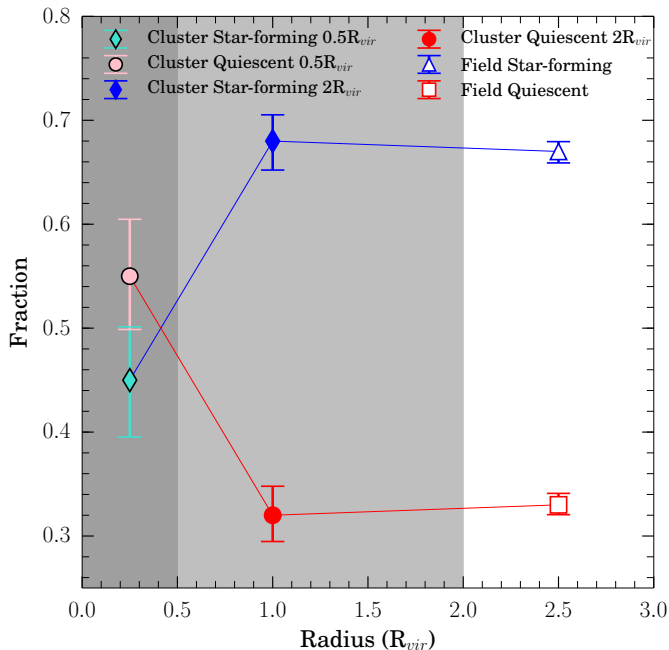


FIG. 4.— The fraction of quiescent (red and pink points) and star-forming galaxies (blue and turquoise points) as a function of cluster radius. The grey contours represent the different radii that samples are chosen from. The fraction of quiescent galaxies increases from 33% to 55% from the field to the cluster core.

analysis of the UVJ color-color selection, as well as confirming passive galaxies at  $z = 3$ . Using rest-frame colors from NMBS, we construct a UVJ color-color diagram for our sample, shown in Figure 3. Galaxies that lie above the relation defined by  $(U - V) > 0.87 \times (V - J) + 0.60$ ,  $(U - V) > 1.3$ , and  $(V - J) < 1.6$  are considered to be quiescent. The total number of star-forming and quiescent galaxies in each sample can be seen in Table 1.

The fraction of star-forming and quiescent galaxies as a function of cluster radius is shown in Figure 4. We calculate the red/blue fractions in our three radius intervals,  $R_{vir} < 0.5$ ,  $0.5 < R_{vir} < 2$ , and  $R_{vir} > 2$ . The error for each fraction is estimated by assuming a beta distribution following Cameron (2011). In the field, the fraction of quiescent galaxies is  $33 \pm 1\%$  compared to star-forming galaxies at  $67 \pm 1\%$ . However, the fraction of quiescent galaxies increases to  $55 \pm 5\%$  within  $0.5R_{vir}$ . The increase of quiescent galaxy fraction as a function of clustocentric distance is suggestive that the density-SFR relation is in place at  $z \sim 1$ . However, we are defining environment using  $R_{vir}$  and not surface-density, therefore we cannot explicitly trace the changes in environmental density.

### 3. ANALYSIS

#### 3.1. Determination of Structural Parameters

We use the CANDELS (Grogin et al. 2011; Koekemoer et al. 2011) *HST*/ACS F814W ( $\lambda \sim 0.42 \mu\text{m}$  rest-frame) image that contains our field and cluster galaxy samples to measure galaxy sizes. The pixel scale of this image is  $0.03''/\text{pixel}$ . We use GALFIT (Peng et al. 2010) to measure the half-light radii of the semi-major axis ( $r_{1/2, \text{maj}}$ ) of each galaxy based on a single Sérsic light profile. GALFIT is run in batch mode, using a python wrapper, on a masked, background subtracted image of each galaxy. Additional inputs for GALFIT include: a point-spread-function (PSF) image, a sigma image, and a constraint file. The constraint file only limits the bounds for the Sérsic index to 0.2–8, Sérsic values above this limit indicate a poor fit (e.g., Raichoor et al. 2012). We explain the process for creating each input below.

Individual galaxy images are created by cutting  $90 \times 90$  pixels, or  $\sim 20 \times 20$  kpc at  $\bar{z} = 0.92$ , thumbnails from the *HST*/ACS F814W image. Each thumbnail has a mask that flags all objects outside of  $1.2''$  from the image centre. We do not mask inside of  $1.2''$  because masking close neighbours to the central galaxy may mask some of the central galaxy's light. Instead, we allow GALFIT to do a multi object fit inside this radius. The masking is accomplished by using SExtractor with a detection threshold of  $2.5\sigma$  above the background rms level to create a bad pixel mask.

We create a sigma image that has a constant value of flux equal to the standard deviation of the flux distribution in the region around the object. The size of the annulus that the flux is measured in has a diameter of  $0.6''$ . The background in each image is estimated from SExtractor and then subtracted from the image using IRAF's IMARITH package.

The use of an accurate PSF is crucial for measuring reliable sizes. We use the PSF image created by the 3DHST survey team (Skelton et al. 2014). For a full description of the construction of the PSF see section 3.3 (and appendix A) of their paper. The FWHM of the PSF is  $0.11''$  ( $\sim 0.9$  kpc at  $\bar{z} = 0.92$ ); we can reliably measure sizes down to  $\text{FWHM}/2$ ,  $\sim 0.5$  kpc (van Dokkum et al. 2010; Straatman et al. 2015a).

After running GALFIT, we exclude galaxies that may

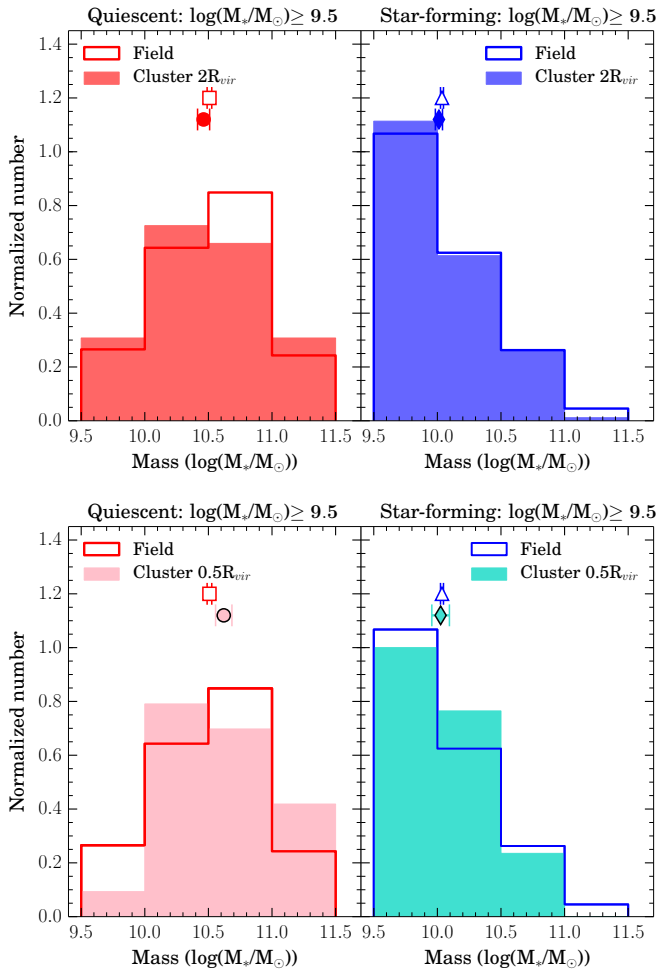


FIG. 5.— Top: Area-normalised mass distributions for quiescent (left) and star-forming (right) field (open histograms) and  $2 R_{vir}$  cluster galaxies (closed histograms). The mass distributions and average masses for quiescent field (open squares) and cluster galaxies (filled circles) are similar and therefore differences in size should not be driven by differences in mass. The mass distributions and average masses for star-forming field (open triangle) and cluster galaxies (filled diamonds) are also consistent. In the bottom panels, area-normalised mass distributions and averages are shown for the  $0.5 R_{vir}$  cluster sample. Again, no significant differences in the mass distributions are seen.

have unreliable measured sizes. Measured galaxy sizes from GALFIT can be unreliable if one or more of the galaxy’s structural parameters is equal to the boundary value given in the constraint file or if they are flagged by GALFIT (see van der Wel et al. 2012). We also remove galaxies if they are unresolved in the NMBS ground based image, but are resolved multicomponent systems in the *HST* image. The fractions of field star-forming and quiescent galaxies that remain after removing galaxies with unreliable sizes are 1189/1397 (85% complete) and 535/690 (78% complete), respectively. For the  $2 R_{vir}$  cluster star-forming and quiescent galaxies the remaining galaxy fractions are 176/206 (85% complete) and 91/97 (94% complete), respectively. The final fractions of  $0.5 R_{vir}$  cluster star-forming and quiescent galaxies are 34/38 (89% complete) and 44/47 (94% complete), respectively. We investigate any possible magnitude or mass dependence of galaxies that fail the GALFIT fitting procedure and find no dependence on mass or magnitude, therefore, these failed fits do not affect our results.

#### 4. RESULTS

##### 4.1. Mass-normalised Sizes

In Figure 5, we show the mass distributions for each sub-sample as well as the average mass. We find that the distributions are similar across environment for the quiescent and star-forming samples. In addition, we use a two-sample KS test to determine if the galaxies in each of the 4 sub-samples shown in Figure 5, are drawn from the same parent sample for each cluster radius and galaxy type. We find that for all sub-samples, field and cluster galaxies are consistent with being drawn from the same parent population all having  $P < 0.14$  or  $< 1.5\sigma$ .

To probe the size differences of field and cluster galaxies, we compare their mass-normalised average sizes (see, Allen et al. 2015, for further details). We fit for average size over the entire size distribution of galaxies using a mass normalisation instead of binning by mass. If field galaxies are not mass-matched to the cluster galaxy sample, then measuring the average size in mass bins can lead to biased results. We fit for the average size as a function of mass using the parametrisation:

$$r(m_*)/\text{kpc} = A \cdot m_*^\alpha \quad (1)$$

For the comparison of the  $2 R_{vir}$  cluster and field galaxy sizes we compute the best fit for both the slope,  $\alpha$ , and y-intercept,  $A$ , of the mass-size relation. Where  $m_*$  is the ratio of the galaxy stellar mass to a constant mass defined below. Errors in the average size and slope are determined from bootstrapping the fit for  $A$  and  $\alpha$ . For the  $0.5 R_{vir}$  cluster and field galaxy average sizes we compute the best fit for  $A$  only, and fix  $\alpha$  to the value obtained in the fit for the  $2 R_{vir}$  cluster and field average sizes. The error in  $A$  is then obtained from bootstrapping.

In Figure 6, we show the mass-size distributions for our sample of quiescent and star-forming, field and cluster galaxies. We show the mass-size relation for both the  $2 R_{vir}$  and  $0.5 R_{vir}$  cluster and field galaxy average sizes (top and bottom panels, respectively). The best-fits and their errors are shown as lines and contours in Figure 6 and are listed in Table 2.

For quiescent galaxies, the mass-size relation flattens at low masses, and can be seen in Figure 6 at  $\log(M_*/M_\odot) \leq 10.3$ . The cause of this flattening may be due to a difference in the projected axis ratios of high and low mass quiescent systems (e.g., Chang et al. 2013). We use the same mass cut as van der Wel et al. (2014), and fit quiescent galaxies with  $\log(M_*/M_\odot) < 10.3$  and  $\log(M_*/M_\odot) > 10.3$  separately, using different values for  $m_*$ . Field and cluster quiescent galaxies with  $\log(M_*/M_\odot) \leq 10.3$ , are fit using  $m_* \equiv M_*/6 \times 10^9 M_\odot$ . We fit field and cluster galaxies with  $\log(M_*/M_\odot) > 10.3$  using  $m_* \equiv M_*/5 \times 10^{10} M_\odot$ .

We find that field and  $2 R_{vir}$  cluster quiescent galaxies with  $\log(M_*/M_\odot) \leq 10.3$  have consistent mass-normalised average sizes. Field and  $2 R_{vir}$  cluster quiescent galaxies with  $\log(M_*/M_\odot) > 10.3$  do not have a significant difference in their average sizes,  $\Delta_{FC} = -0.14 \pm 0.11$  ( $1.27\sigma$ ), and we can rule out any size difference greater than 6%. The best-fits for  $A$  and  $\alpha$  are listed in Table 2, and the mass-normalised sizes that correspond to these fits are shown in Table 3.

The mass-normalised average sizes for field and  $0.5 R_{vir}$  cluster quiescent galaxies remain consistent at masses above and below  $\log(M_*/M_\odot) = 10.3$ . The lack of any significant size difference between field and cluster quiescent galaxies, regardless of cluster distance, indicates that environment is not accelerating their size growth.

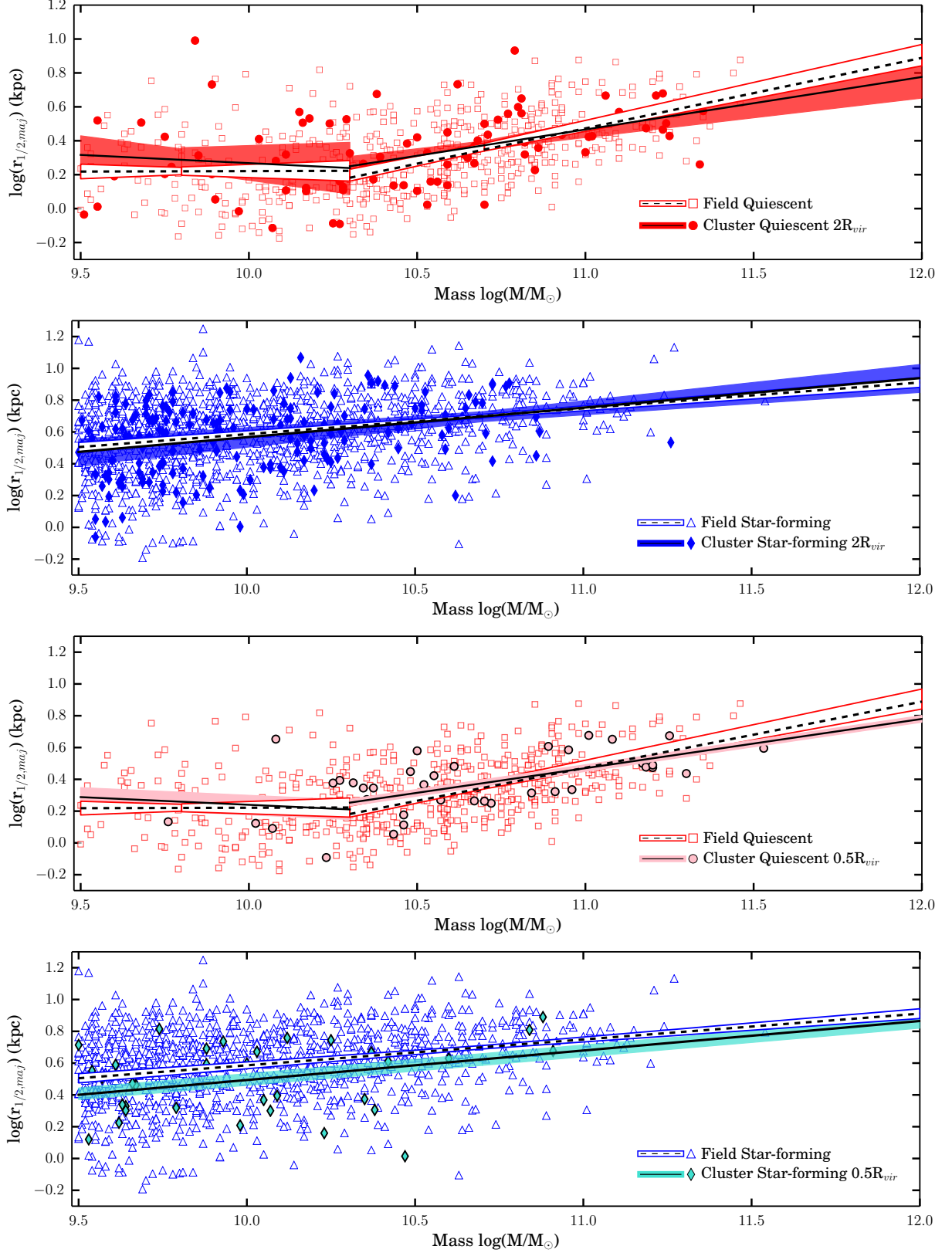


FIG. 6.— mass–size distributions for quiescent and star-forming, field and cluster galaxies. In all panels, the field star-forming and quiescent galaxies are represented by open blue triangles and red squares, respectively. In the top two panels, the cluster samples are selected within  $2 R_{vir}$  and are shown as solid blue diamonds (star-forming) or solid red squares (quiescent). The best-fits to the data are shown as solid (dashed) lines for cluster and field galaxies. The respective bootstrap errors for these fits are shown as filled (open) contours. The best-fits, their bootstrap errors, and average sizes are shown in Table 2 and Table 3. The best-fit for field and  $2 R_{vir}$  cluster quiescent galaxies with  $\log(M_*/M_\odot) > 10.3$  are consistent. The best-fits are consistent for field and  $2 R_{vir}$  cluster star-forming galaxies. The bottom two panels are the same, except the cluster samples are selected with  $0.5 R_{vir}$  and the colors of the symbols are a lighter color. The slope is fixed to the best-fit value obtained from the  $2 R_{vir}$  fits for each environment and galaxy type. For cluster galaxies within  $0.5 R_{vir}$ , the mass–normalised average size for field and cluster quiescent galaxies remain roughly consistent. However, the mass–normalised average size for star-forming field galaxies is  $16 \pm 7\%$  larger than that of star-forming  $0.5 R_{vir}$  cluster galaxies.

TABLE 2  
BEST-FIT VALUES FOR  $A$  AND  $\alpha$  TO DETERMINE THE MASS-NORMALISED AVERAGE SIZES OF THE FORM:  
 $r(m_*)/kpc = A \cdot m_*^\alpha$ , WHERE  $m_* \equiv M_*/5 \times 10^{10} M_\odot$

| Environment                            | Quiescent <sup>1</sup> |                 | Star-forming    |                 |
|--|------------------------|-----------------|-----------------|-----------------|
|  | log( $A$ )             | $\alpha$        | log( $A$ )      | $\alpha$        |
| Field                                  | $0.35 \pm 0.01$        | $0.42 \pm 0.03$ | $0.70 \pm 0.01$ | $0.16 \pm 0.02$ |
| Cluster ( $2 R_{vir}$ )                | $0.37 \pm 0.03$        | $0.31 \pm 0.08$ | $0.70 \pm 0.03$ | $0.19 \pm 0.04$ |
| Cluster ( $0.5 R_{vir}$ ) <sup>2</sup> | $0.38 \pm 0.02$        | –               | $0.62 \pm 0.04$ | –               |

<sup>1</sup> Fits are only shown for galaxies with  $\log(M_*/M_\odot) > 10.3$

<sup>2</sup>  $\alpha$  is fixed to the  $2 R_{vir}$  value

TABLE 3  
SÉRSIC INDICES AND MASS-NORMALISED AVERAGE SIZES OF STAR-FORMING AND QUIESCENT  
FIELD AND CLUSTER GALAXIES DERIVED FROM *HST*/ACS F814W IMAGES

| Environment                     | Quiescent <sup>1</sup>            |                                   | Star-forming                     |                                   |
|---------------------------------|-----------------------------------|-----------------------------------|----------------------------------|-----------------------------------|
|                                 | $r_{1/2,maj}$<br>(kpc)            | $n$                               | $r_{1/2,maj}$<br>(kpc)           | $n$                               |
| Field                           | $2.23 \pm 0.04$                   | $1.96 \pm 0.03$                   | $5.01 \pm 0.13$                  | $0.94 \pm 0.02$                   |
| Cluster ( $2 R_{vir}$ )         | $2.36 \pm 0.13$                   | $1.96 \pm 0.07$                   | $4.98 \pm 0.37$                  | $0.92 \pm 0.04$                   |
| Cluster ( $0.5 R_{vir}$ )       | $2.38 \pm 0.11$                   | $2.05 \pm 0.07$                   | $4.20 \pm 0.36$                  | $1.22 \pm 0.11$                   |
| $\Delta_{FC}^2$ ( $2 R_{vir}$ ) | $-0.13 \pm 0.14$ ( $0.9\sigma$ )  | $0.0 \pm 0.08$ ( $0\sigma$ )      | $0.03 \pm 0.39$ ( $0.08\sigma$ ) | $-0.02 \pm 0.04$ ( $0.22\sigma$ ) |
| $\Delta_{FC}$ ( $0.5 R_{vir}$ ) | $-0.15 \pm 0.12$ ( $1.25\sigma$ ) | $-0.09 \pm 0.08$ ( $1.12\sigma$ ) | $0.81 \pm 0.38$ ( $2.20\sigma$ ) | $-0.28 \pm 0.11$ ( $2.5\sigma$ )  |

<sup>1</sup> Sizes and Sérsic indices are for galaxies with  $\log(M_*/M_\odot) > 10.3$

<sup>2</sup>  $\Delta_{FC} \equiv \text{Field} - \text{Cluster}$



We fit star-forming galaxies with  $\log(M_*/M_\odot) > 9.5$  using  $m_* \equiv M_*/5 \times 10^{10} M_\odot$ . Field and  $2 R_{vir}$  cluster star-forming galaxies have consistent mass-normalised average sizes,  $\Delta_{FC} = 0.03 \pm 0.39$  ( $0.08\sigma$ ). However, the average size for field star-forming galaxies is  $16 \pm 7\%$  larger than that of  $0.5 R_{vir}$  cluster star-forming galaxies,  $\Delta_{FC} = 0.81 \pm 0.38$  ( $2.20\sigma$ ). This result remains even if we do not fix the slope. The smaller sizes we find for  $0.5 R_{vir}$  star-forming galaxies suggests that environment is either acting on their growth mechanisms, i.e., quenching their SFRs and stunting their growth, or disrupting their stellar disks and truncating their light profiles.

Different from some studies, we have selected our sample using UVJ colors. We now test if selecting by Sérsic index/morphology (e.g., Kauffmann et al. 2004; Newman et al. 2014; Kelkar et al. 2015) affects our results. We reselect our samples of galaxies with  $n$  above and below  $n = 2.5$ , and refit the sizes. We find that there is no significant change in our results.

#### 4.2. Sérsic indices

In Figure 7, we show the area-normalised distribution of Sérsic indices and their averages for field and cluster, star-forming and quiescent galaxies obtained from GALFIT. Errors in the average values are estimated using the error in the mean.

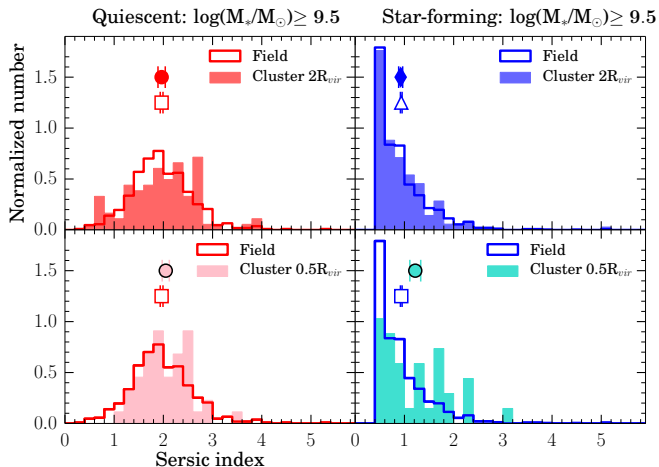


FIG. 7.— Area-normalised distributions of the Sérsic indices of quiescent (left) and star-forming (right) field (open histograms) and cluster (closed histograms) galaxies. The top panels are for the cluster samples drawn within apertures of  $2 R_{vir}$ . The distributions of Sérsic index for field and cluster quiescent galaxies are consistent. The same is true for star-forming galaxies. The bottom two panels are the same except the cluster sample aperture is  $0.5 R_{vir}$ . Quiescent galaxies remain consistent in distributions of  $n$ , however, the fraction of star-forming galaxies with  $n > 1$  is 0.5 in the cluster core compared to 0.31 for field star-forming galaxies.

In Table 3, we show these averages and their errors as well as the significance of their difference between field and cluster. The top panels of Figure 7 are for  $2 R_{vir}$  cluster galaxies while the bottom panels are for  $0.5 R_{vir}$  cluster galaxies. The distribution of Sérsic indices for both field and cluster quiescent galaxies, regardless of cluster-centric radius. The fraction of quiescent field galaxies with  $n > 2$  is 0.42, compared to 0.52 for the cluster outskirts, and 0.49 for the cluster core. Where the average Sérsic index for field quiescent galaxies is  $1.96 \pm 0.03$  compared to the cluster outskirts,  $n = 1.96 \pm 0.07$ , and cluster core,  $n = 2.05 \pm 0.07$ . The lack of

a difference in the distributions or averages in Sérsic index for field and cluster quiescent galaxies, regardless of cluster distance, suggests that these galaxies are most likely similar in morphologies, and we cannot use Sérsic index to differentiate their growth mechanisms.

The distributions of Sérsic indices and the average Sérsic index of field and cluster star-forming galaxies at  $2 R_{vir}$  are consistent. We do note, however, that the  $0.5 R_{vir}$  cluster galaxies have a different distribution of  $n$  relative to the field galaxies. Galaxies within  $0.5 R_{vir}$  have an equal fraction of  $n > 1$  and  $n < 1$  Sérsic indices. This is in stark contrast to the field, where the fraction of galaxies with  $n < 1$  is 0.69, see Figure 7. The distribution in Sérsic indices of the cluster core galaxies could be indicative of a distribution in spectral types, as observed in Abramson et al. (2013), while the field star-forming population may be more uniform.

#### 4.3. Star-Formation Rates

By comparing the SFRs of field and cluster, star-forming galaxies we can quantify possible differential growth. We use the SFRs from the NMBS UV+IR SFR catalog for individual galaxies. For more details on the derivation of SFRs, please see Whitaker et al. (2012b).

Because there is a known trend of increasing SFR with mass (e.g., Brinchmann et al. 2004; Peng et al. 2010), we compare SFRs between field and cluster by determining mass-normalised average SFRs. We fit the mass-SFR relations using the same parameterisation used to fit our mass-size relations. Again, we use  $m_* \equiv M_*/5 \times 10^{10} M_\odot$  for galaxies with  $\log(M_*/M_\odot) > 9.5$ .

In Figure 8, we show the mass-SFR distributions and their best-fits for our samples of star-forming galaxies. The error in the average SFR is derived by bootstrapping the fit, and can be seen in Figure 8 as filled and open contours. The average SFRs, their errors, and the significance at which they differ from each other can be seen in Table 4. Field galaxies have an average SFR of  $26.4 \pm 1.1 \text{ yr}^{-1}$  compared to  $11.9 \pm 1.9 \text{ yr}^{-1}$  for the cluster outskirts and  $10.0 \pm 1.4 \text{ yr}^{-1}$  for the cluster core. While this difference has a significance of  $7-9\sigma$ , it can be seen in Figure 9, that the larger difference in SFR between field and cluster occurs for galaxies with  $\log(M_*/M_\odot) > 10.3$ . Therefore, it is likely that the higher mass galaxies drive the difference in SFRs, and that the cluster environment is effective at suppressing or quenching the star-formation of massive galaxies, while lower mass cluster and field galaxies have similar SFRs.

In Figure 9, we show the mass-normalised average SFRs as a function of clustocentric radius. The average SFR drops by a factor of two within  $2 R_{vir}$ , however, the the average SFRs between the cluster outskirts and core are consistent, suggesting that environmental effects extend to  $2 R_{vir}$ .

## 5. DISCUSSION

We have used a sample of star-forming and quiescent, field and cluster galaxies at  $\bar{z} = 0.92$  to study the influence of environment on galaxy properties. For the first time, we use different values of  $R_{vir}$  to probe the effects of environment on galaxy sizes. It appears that only the star-forming galaxies found within  $0.5 R_{vir}$  of the cluster centres show a significant difference in size and Sérsic index compared to their field counter-parts at  $\bar{z} = 0.92$ . The difference of these two populations is further supported by the suppressed SFRs of cluster star-forming galaxies compared to field star-forming galaxies. On the other hand, quiescent field and cluster galaxies

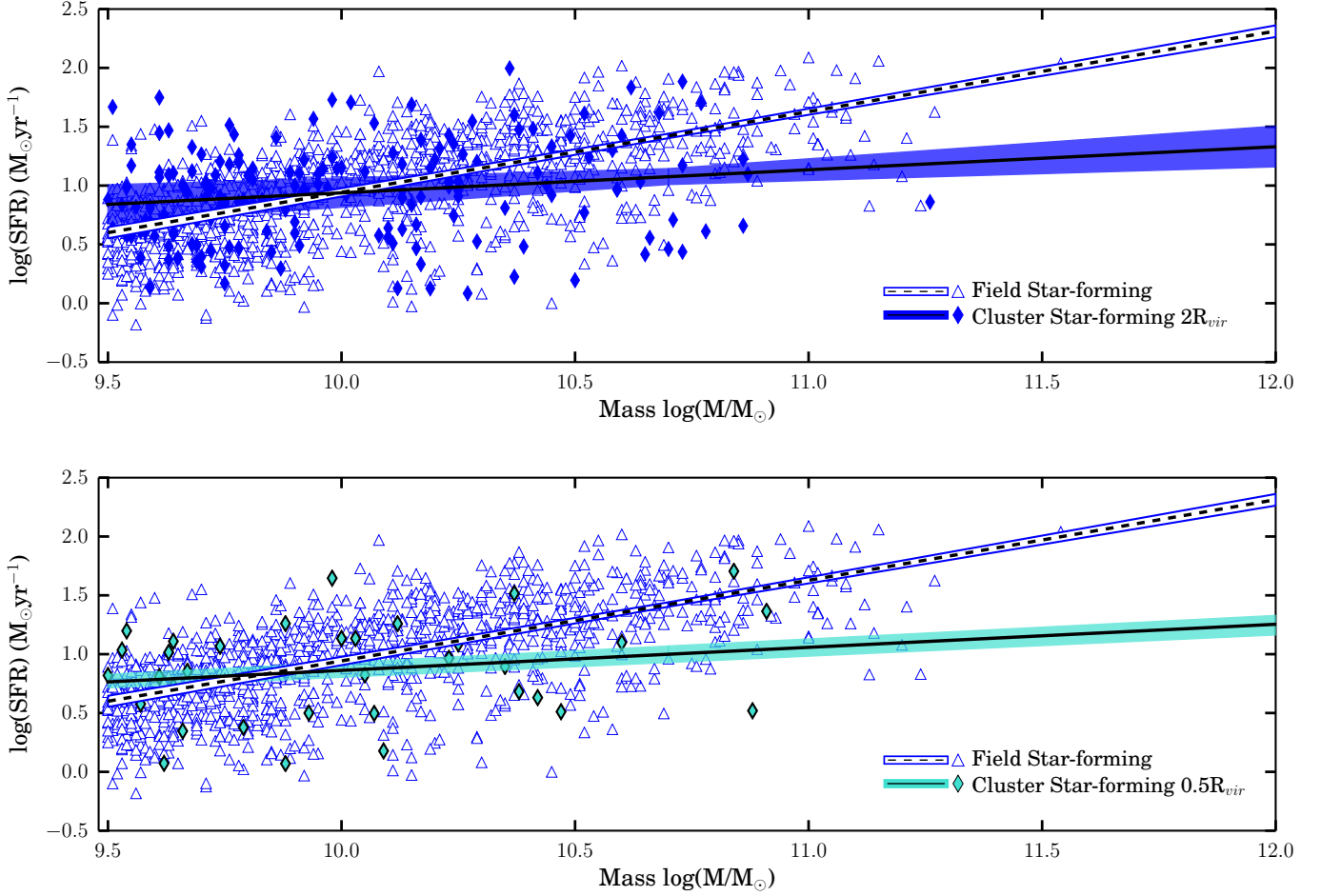


FIG. 8.— Mass–SFR distributions for star-forming, field and cluster galaxies. In both panels, the field star-forming galaxies are represented by open blue triangles. In the top panel, the cluster samples are selected within  $2 R_{vir}$  and are shown as solid blue diamonds. In the bottom panel, we show cluster galaxies chosen within  $0.5 R_{vir}$  as turquoise diamonds. The best-fits to the mass–SFR distributions are shown as solid (dashed) lines for cluster and field galaxies. The respective bootstrap errors for these fits are shown as filled (open) contours. The derived average sizes and their errors are shown in Table 4. The best-fits for the field and cluster galaxies are different by  $\sim 8\sigma$ , indicating that the cluster galaxies are undergoing quenching.

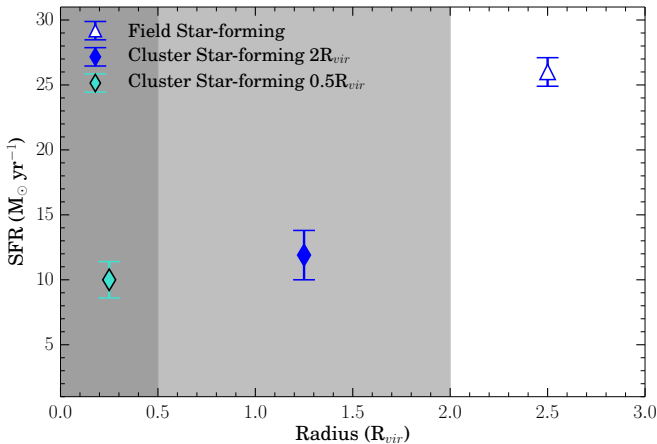


FIG. 9.— Mass-normalised average star-formation rates (SFR) for field and cluster star-forming galaxies as a function of  $R_{vir}$ . The averages are measured within three cluster-centric distances of  $0-0.5 R_{vir}$ ,  $0.5-2 R_{vir}$ , and  $> 2 R_{vir}$ . Errors are calculated from bootstrapping the fit to the mass–SFR relation from Figure 8. The average SFR of field star-forming galaxies is up to 2.5 times larger than that of the cluster. This indicates that the environment is likely quenching galaxies.

have consistent sizes Sérsic indices, and SFRs, independent of cluster-centric radius.

TABLE 4  
MASS-NORMALISED SFRs FOR FIELD AND CLUSTER STAR-FORMING GALAXIES. SFRs HAVE UNITS OF  $M_{\odot} \text{ YR}^{-1}$ .

| Environment                   | SFR                        |
|-------------------------------|----------------------------|
| Field                         | $26.4 \pm 1.1$             |
| Cluster ( $2 R_{vir}$ )       | $11.9 \pm 1.9$             |
| Cluster ( $0.5 R_{vir}$ )     | $10.0 \pm 1.4$             |
| $\Delta_{FC}^1 (2 R_{vir})$   | $14.5 \pm 2.2 (6.6\sigma)$ |
| $\Delta_{FC}^1 (0.5 R_{vir})$ | $16.4 \pm 1.8 (9.2\sigma)$ |

<sup>1</sup>  $\Delta_{FC} \equiv \text{Field} - \text{Cluster}$

### 5.1. Quiescent Galaxies

We do not find any significant difference between the sizes and Sérsic indices of field and cluster quiescent galaxies; therefore, we can infer that they are evolving similarly. This result is consistent with other studies regardless of sample selection or redshift (e.g., Huertas-Company et al. 2013b; Newman et al. 2014; Allen et al. 2015; Kelkar et al. 2015). To illustrate this, we plot the difference in  $r_{1/2, \text{maj}}$  between field and cluster quiescent galaxies at several redshifts, see Figure 10. We adopted this approach from Newman et al. (2014) and use their data and as well as the work of this study, Allen et al. (2015), Cebrían & Trujillo (2014), and Kelkar et al. (2015).

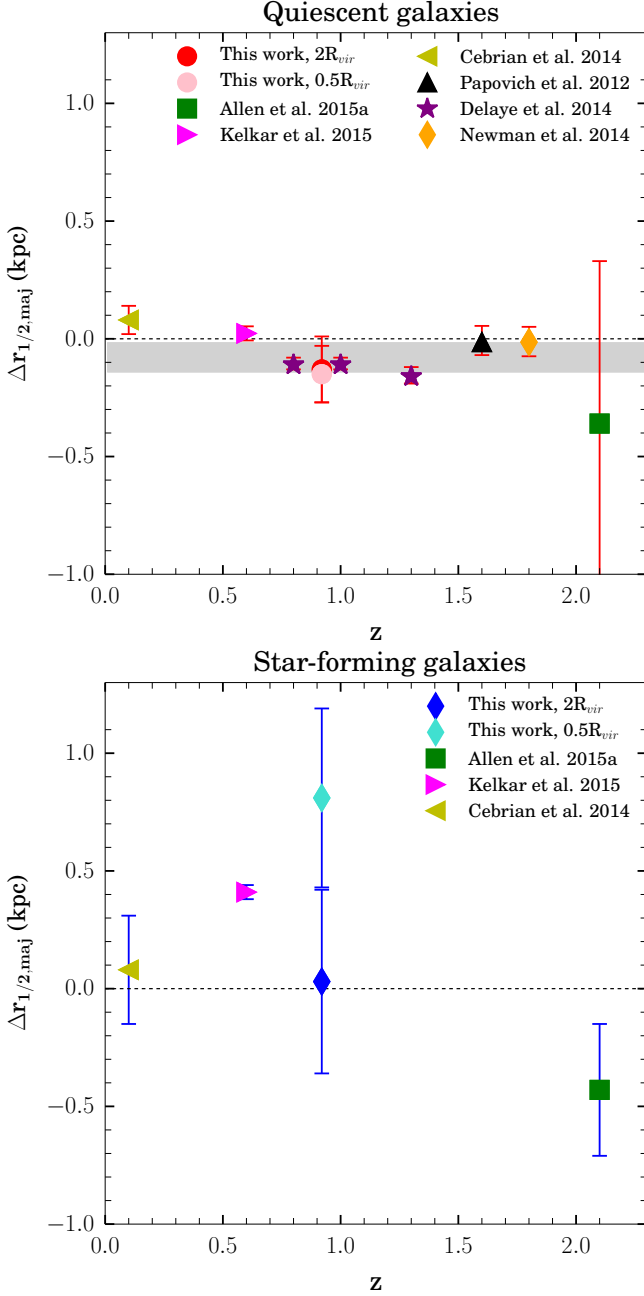


FIG. 10.— The evolution of  $\Delta r_{1/2,maj}$  between the field and cluster for quiescent galaxies (top panel) and star-forming galaxies (bottom panel).  $\Delta r_{1/2,maj}$  is the difference of  $r_{1/2,maj}$  field minus  $r_{1/2,maj}$  cluster. Our data are shown as red and pink filled circles (quiescent galaxies,  $0.5 R_{vir}$  and  $2 R_{vir}$ , respectively) and blue and turquoise filled diamonds (star-forming galaxies,  $0.5 R_{vir}$  and  $2 R_{vir}$ , respectively). We show a linear fit to the data, including one sigma errors, as a grey contour (the slope is fixed to zero) for quiescent galaxies. We weight the contribution of each point to the fit by its errors. The difference we measure for quiescent galaxies is marginal,  $\Delta r_{1/2,maj} = -0.09 \pm 0.06$ .

When we assume zero slope and preform a linear fit to the data we find an average difference of  $-0.09 \pm 0.06$  kpc ( $< 2 \sigma$ ) between the sizes of field and cluster quiescent galaxies. For an average quiescent cluster galaxy with  $\log(M_*/M_\odot)=10.7$  and  $r_{1/2,maj} = 2.4$  kpc, this difference would only represent a size offset of 4% from a field quiescent galaxy with the same mass. We conclude that environment does not affect the size evolution of quiescent galaxies.

The two data points from Delaye et al. (2014) deviate from zero size difference by a significant amount (see Figure 10). The halo masses of the clusters in their study are on the order of  $M_h \sim 10^{15} M_\odot$  where those in our work are on the order of  $M_h \sim 10^{13-14} M_\odot$ . Larger sizes are expected for cluster galaxies that reside in larger mass halos (e.g., Shankar et al. 2014), therefore, the lack of size difference measured in our work could be due to the lower mass halos of our clusters.

While it seems that there is little to no size difference between field and cluster quiescent galaxies, more studies are needed that consider the effects of different mass halos and different cluster-centric radii to constrain this apparent lack of environmental effects.

## 5.2. Star-forming Galaxies

We found no significant difference between the sizes and Sérsic indices of star-forming galaxies in the outer cluster region ( $2 > R_{vir} > 0.5$ ) and field. However, within the cluster core ( $R_{vir} < 0.5$ ), star-forming galaxies have smaller sizes and Sérsic indices with equal frequency above and below  $n = 1$ , compared to the field. Here, we explore what phenomena would cause environment to have a significant effect on star-forming galaxy sizes at  $R_{vir} < 0.5$ , and star-forming galaxy SFRs within  $2 R_{vir}$ .

The smaller sizes of the cluster core galaxies may be due to a combination of tidal stripping and harassment. Therefore, a difference in dynamical timescales of galaxies that reside in the outer cluster regions versus the cluster core could explain the difference in their structural properties. We use the velocity dispersions calculated in Balogh et al. (2014) to estimate the different dynamical times,  $t_{dyn}$ , as a function of  $R_{vir}$  for galaxies in this study. Galaxies in the outer cluster have  $t_{dyn} \sim 3.4$  Gyr compared to  $t_{dyn} \sim 1.7$  Gyr for galaxies in the cluster core. Therefore, galaxies in the cluster core have most likely been exposed to environmental effects such as tidal stripping and harassment more frequently than those in the outer cluster.

Environmental effects would also cause suppressed star-formation that could be contributing to the smaller sizes (in rest-frame B-band). This is consistent with our results where the average SFR of the core is a factor of 2.5 lower than the field. However, the average SFR of the cluster outskirts is also suppressed compared to the field, but the average sizes between the outskirts and field are consistent. This may be a result of a timescale issue where galaxies in the cluster outskirts have begun to quench, but that is not yet reflected in their sizes. This is consistent with Wetzel et al. (2013) who found that satellite galaxies remain star-forming for 2–4 Gyr after their first cluster infall and then rapidly quench. Furthermore, the difference in SFR between the field and cluster is likely driven by galaxies with  $\log(M_*/M_\odot) > 10.3$ , while the SFRs of lower mass galaxies are similar regardless of environment. This is consistent with previous studies that find higher quenching efficiencies and lower specific SFRs for massive star-forming galaxies in groups (e.g., Lin et al. 2014). Therefore, it is likely that environmental effects extend to  $2 R_{vir}$ , however, the timescale for which a difference in size can be seen is longer than for the cluster core.

There are few studies that compare the sizes of field and cluster star-forming galaxies at any redshift. In Figure 10, we show all of the current studies that measure the size difference for field and cluster star-forming galaxies. From these few results it is unclear what role environment plays in the growth of

star-forming galaxies. To understand what is driving this size difference in the cores of clusters at  $\bar{z} = 0.92$  and if it is occurring at lower or high redshifts, more studies that consider the effects of environment as a function of  $R_{vir}$  are needed.

While we chose to use clustocentric distance to define environment, it has been shown that surface density more strongly traces changes in galaxy populations in over-dense environments, such as spectral type and Sérsic index (Abramson et al. 2013; Dressler et al. 2013). To really understand how clusters affect their galaxies, it is important to understand how both environmental density and clustocentric radius play a role.

## 6. CONCLUSIONS

We have studied the dependence of the mass–size relation on environment at different intervals of cluster  $R_{vir}$  using  $\sim 2400$  field and cluster galaxies at  $\bar{z} = 0.92$ . From the GEEC2 and NMBS surveys, we utilised accurate rest frame colors and stellar masses to select our mass-complete sample (down to  $\log(M_*/M_\odot) \geq 9.5$ ) of star-forming and quiescent galaxies. Our main results are as follows.

For quiescent galaxies:

- We rule out a size difference of more than 6%, regardless of the cluster-centric radius. Combining previous results from the literature, we determine that quiescent cluster galaxies are at most  $0.09 \pm 0.06$  kpc larger in size than their field counter-parts.
- Field and cluster galaxies are consistent in Sérsic index, regardless of the cluster-centric radius.

For star-forming galaxies:

- We find that the mass normalised ( $\log(M_*/M_\odot) = 10.7$ ) average size of cluster star-forming galaxies within  $0.5 R_{vir}$  is  $16 \pm 7\%$  smaller, than field star-forming galaxies. However, this difference disappears if cluster star-forming galaxies are at a larger radius of  $2 R_{vir}$ .
- The fraction of galaxies with Sérsic indices with  $n > 1$  for cluster star-forming galaxies within  $0.5 R_{vir}$  is 50% compared to a fraction of 30 for field star-forming

galaxies. Again, this difference disappears for a cluster sample at larger radius.

- The mass-normalised average SFR of field star-forming galaxies is elevated by a factor of 2 (significance of  $7-9\sigma$ ) compared to cluster star-forming galaxies, regardless of clustocentric radius. However, this trend appears to be driven by the high mass end, indicating that environment is more efficient at quenching galaxies with  $\log(M_*/M_\odot) > 10.3$ .

Our results are consistent with previous works which all show that the dependence of the mass–size relation on environment for quiescent galaxies is minimal at best. This continues to be surprising because quiescent galaxies are thought to be built up via mergers which should occur more frequently in clusters. These mergers are likely responsible, at least in part, for producing the morphology-density relation. It is, however, clear that the cluster environment plays an important role controlling the gas content of galaxies. Thus, perhaps it is more useful to study star-forming galaxies where environment can have its greatest effect on gas content, SFRs and sizes and possibly transition active galaxies into passive ones.

While there are few studies that examine the mass–size relation of star-forming galaxies as a function of redshift, we can use those results to infer that environment does appear to influence the size of star-forming galaxies. The lower average SFRs of cluster star-forming galaxies could mean that they have lost access to cold gas reservoirs in the cluster core and cannot grow via star-formation at the same rate as galaxies in the field. Additional studies are needed to constrain the effects of environment on the growth mechanisms of star-forming galaxies, preferentially spanning  $0 \leq z \leq 3$  so that it is clear at what epoch massive cluster star-forming galaxies are becoming quenched.

We thank the referee for their comprehensive and constructive comments. Research support to R.J.A is provided by the Australian Astronomical Observatory. G.G.K acknowledges the support of the Australian Research Council through the award of a Future Fellowship (FT140100933). K.G. acknowledges funding from the Australian Research Council (ARC) Discovery Program (DP) grant DP1094370.

## REFERENCES

- Abramson, L. E., Dressler, A., Gladders, M. D., et al. 2013, *ApJ*, 777, 124  
 Allen, R. J., Kacprzak, G. G., Spitler, L. R., et al. 2015, *ApJ*, 806, 3  
 Balogh, M. L., McGee, S. L., Mok, A., et al. 2014, *MNRAS*, 443, 2679  
 Barden, M., Rix, H.-W., Somerville, R. S., et al. 2005, *ApJ*, 635, 959  
 Bassett, R., Papovich, C., Lotz, J. M., et al. 2013, *ApJ*, 770, 58  
 Belli, S., Newman, A. B., & Ellis, R. S. 2014, *ApJ*, 783, 117  
 Bertin, E., & Armouts, S. 1996, *A&AS*, 117, 393  
 Bouché, N., Murphy, M. T., Kacprzak, G. G., et al. 2013, *Science*, 341, 50  
 Brammer, G. B., van Dokkum, P. G., & Coppi, P. 2008, *ApJ*, 686, 1503  
 Brinchmann, J., Charlot, S., White, S. D. M., et al. 2004, *MNRAS*, 351, 1151  
 Bruzual, G. & Charlot, S. 2003, *MNRAS*, 344, 1000  
 Cameron, E. 2011, *PASA*, 28, 128  
 Capak, P., Aussel, H., Ajiki, M., et al. 2007, *ApJS*, 172, 99  
 Cebrián, M., & Trujillo, I. 2014, *MNRAS*, 444, 682  
 Chang, Y.-Y., van der Wel, A., Rix, H.-W., et al. 2013, *ApJ*, 773, 149  
 Cimatti, A., Nipoti, C., & Cassata, P. 2012, *MNRAS*, 422, L62  
 Cooper, M. C., Griffith, R. L., Newman, J. A., et al. 2012, *MNRAS*, 419, 3018  
 Cooper, M. C., Newman, J. A., Weiner, B. J., et al. 2008, *MNRAS*, 383, 1058  
 Cowley, M. J., Spitler, L. R., Tran, K.-V. H., et al. 2016, *MNRAS*, 457, 629  
 Delaye, L., Huertas-Company, M., Mei, S., et al. 2014, *MNRAS*, 441, 203  
 Dénes, H., Kilborn, V. A., Koribalski, B. S., & Wong, O. I. 2016, *MNRAS*, 455, 1294  
 Dressler, A., Oemler, A., Jr., Poggianti, B. M., et al. 2013, *ApJ*, 770, 62  
 Dressler, A., Oemler, A., Jr., Couch, W. J., et al. 1997, *ApJ*, 490, 577  
 Dressler, A. 1980, *ApJ*, 236, 351  
 Fan, L., Lapi, A., Bressan, A., et al. 2010, *ApJ*, 718, 1460  
 Fan, L., Lapi, A., De Zotti, G., & Danese, L. 2008, *ApJ*, 689, L101  
 George, M. R., Leauthaud, A., Bundy, K., et al. 2011, *ApJ*, 742, 125  
 Grogin, N. A., Kocevski, D. D., Faber, S. M., et al. 2011, *ApJS*, 197, 35  
 Gunn, J. E., & Gott, J. R., III 1972, *ApJ*, 176, 1  
 Guo, Q., White, S., Boylan-Kolchin, M., et al. 2011, *MNRAS*, 413, 101  
 Hansen, S. M., Sheldon, E. S., Wechsler, R. H., & Koester, B. P. 2009, *ApJ*, 699, 1333  
 Hilton, M., Lloyd-Davies, E., Stanford, S. A., et al. 2010, *ApJ*, 718, 133  
 Hiltz, M., Naab, T., & Ostriker, J. P. 2013, *MNRAS*, 429, 2924  
 Huertas-Company, M., Mei, S., Shankar, F., et al. 2013, *MNRAS*, 428, 1715  
 Huertas-Company, M., Shankar, F., Mei, S., et al. 2013, *ApJ*, 779, 29  
 Kauffmann, G., White, S. D. M., Heckman, T. M., et al. 2004, *MNRAS*, 353, 713  
 Kelkar, K., Aragón-Salamanca, A., Gray, M. E., et al. 2015, *MNRAS*, 450, 1246

- Khochfar, S., & Silk, J. 2006, *ApJ*, 648, L21
- Koekemoer, A. M., Faber, S. M., Ferguson, H. C., et al. 2011, *ApJS*, 197, 36
- Kriek, M., van Dokkum, P. G., Whitaker, K. E., et al. 2011, *ApJ*, 743, 168
- Kriek, M., van Dokkum, P. G., Labbe, I., et al. 2009, *ApJ*, 700, 221
- Labbé, I., Huang, J., Franx, M., et al. 2005, *ApJ*, 624, L81
- Lang, P., Wuyts, S., Somerville, R. S., et al. 2014, *ApJ*, 788, 11
- Lani, C., Almaini, O., Hartley, W. G., et al. 2013, *MNRAS*, 435, 207
- Lemaux, B. C., Cucciati, O., Tasca, L. A. M., et al. 2014, *A&A*, 572, A41
- Lemaux, B. C., Gal, R. R., Lubin, L. M., et al. 2012, *ApJ*, 745, 106
- L'Huillier, B., Combes, F., & Semelin, B. 2012, *A&A*, 544, A68
- Lilly, S. J., Le Fèvre, O., Renzini, A., et al. 2007, *ApJS*, 172, 70
- Lin, L., Jian, H.-Y., Foucaud, S., et al. 2014, *ApJ*, 782, 33
- McLure, R. J., Pearce, H. J., Dunlop, J. S., et al. 2013, *MNRAS*, 428, 1088
- Mei, S., Scarlata, C., Pentericci, L., et al. 2015, *ApJ*, 804, 117
- Moran, S. M., Ellis, R. S., Treu, T., & Smith, G. P. 2007, *Cosmic Frontiers*, 379, 243
- Morishita, T., Ichikawa, T., & Kajisawa, M. 2014, *ApJ*, 785, 18
- Naab, T., Johansson, P. H., & Ostriker, J. P. 2009, *ApJ*, 699, L178
- Newman, A. B., Ellis, R. S., Andreon, S., et al. 2014, *ApJ*, 788, 51
- Newman, A. B., Ellis, R. S., Bundy, K., & Treu, T. 2012, *ApJ*, 746, 162
- 2013ApJ...770...58B Papovich, C., Bassett, R., Lotz, J. M., et al. 2012, *ApJ*, 750, 93
- Papovich, C., Labbé, I., Quadri, R., et al. 2015, *ApJ*, 803, 26
- Patel, S. G., van Dokkum, P. G., Franx, M., et al. 2013, *ApJ*, 766, 15
- Patel, S. G., Holden, B. P., Kelson, D. D., et al. 2012, *ApJ*, 748, L27
- Patel, S. G., Kelson, D. D., Holden, B. P., Franx, M., & Illingworth, G. D. 2011, *ApJ*, 735, 53
- Peng, Y.-j., Lilly, S. J., Kovač, K., et al. 2010, *ApJ*, 721, 193
- Postman, M., Franx, M., Cross, N. J. G., et al. 2005, *ApJ*, 623, 721
- Quadri, R. F., Williams, R. J., Franx, M., & Hildebrandt, H. 2012, *ApJ*, 744, 88
- Raichoor, A., Mei, S., Stanford, S. A., et al. 2012, *ApJ*, 745, 130
- Scoville, N. 2007, *From Z-Machines to ALMA: (Sub)Millimeter Spectroscopy of Galaxies*, 375, 166
- Shankar, F., Buchan, S., Rettura, A., et al. 2015, *ApJ*, 802, 73
- Shankar, F., Mei, S., Huertas-Company, M., et al. 2014, *MNRAS*, 439, 3189
- Szomoru, D., Franx, M., van Dokkum, P. G., et al. 2013, *ApJ*, 763, 73
- Straatman, C. M. S., Labbé, I., Spitler, L. R., et al. 2015, *ApJ*, 808, L29
- Straatman, C. M. S., A. R., Quadri, Labbe, I., Spitler, L. R., et al. 2015, submitted to *ApJ*
- Skelton, R. E., Whitaker, K. E., Momcheva, I. G., et al. 2014, *ApJS*, 214, 24
- Spitler, L. R., Labbé, I., Glazebrook, K., et al. 2012, *ApJ*, 748, L21
- Tilvi, V., Papovich, C., Tran, K.-V. H., et al. 2013, *ApJ*, 768, 56
- Tomczak, A. R., Quadri, R. F., Tran, K.-V. H., et al. 2014, *ApJ*, 783, 85
- Tran, K.-V. H., Papovich, C., Saintonge, A., et al. 2010, *ApJ*, 719, L126
- Tran, K.-V. H., Saintonge, A., Moustakas, J., et al. 2009, *ApJ*, 705, 809
- Treu, T., Ellis, R. S., Kneib, J.-P., et al. 2003, *ApJ*, 591, 53
- Trujillo, I., Conselice, C. J., Bundy, K., et al. 2007, *MNRAS*, 382, 109
- van der Wel, A., Franx, M., van Dokkum, P. G., et al. 2014, *ApJ*, 788, 28
- van der Wel, A., Bell, E. F., Häussler, B., et al. 2012, *ApJS*, 203, 24
- van Dokkum, P. G., Whitaker, K. E., Brammer, G., et al. 2010, *ApJ*, 709, 1018
- Wetzel, A. R., Tinker, J. L., Conroy, C., & van den Bosch, F. C. 2013, *MNRAS*, 432, 336
- Wetzel, A. R., Tinker, J. L., & Conroy, C. 2012, *MNRAS*, 424, 232
- Whitaker, K. E., van Dokkum, P. G., Brammer, G., & Franx, M. 2012, *ApJ*, 754, L29
- Whitaker, K. E., Kriek, M., van Dokkum, P. G., et al. 2012, *ApJ*, 745, 179
- Whitaker, K. E., Labbé, I., van Dokkum, P. G., et al. 2011, *ApJ*, 735, 86
- Wild, V., Almaini, O., Cirasuolo, M., et al. 2014, *MNRAS*, 440, 1880
- Williams, R. J., Quadri, R. F., Franx, M., van Dokkum, P., & Labbé, I. 2009, *ApJ*, 691, 1879
- Wuyts, S., Förster Schreiber, N. M., van der Wel, A., et al. 2011, *ApJ*, 742, 96
- Wuyts, S., van Dokkum, P. G., Franx, M., et al. 2009, *ApJ*, 706, 885
- Yuan, T., Nanayakkara, T., Kacprzak, G. G., et al. 2014, *ApJ*, 795, LL20
- Zeimann, G. R., Stanford, S. A., Brodwin, M., et al. 2013, *ApJ*, 779, 137